Available online at www.sciencedirect.com
ScienceDirect
Energy Conversion and Management 49 (2008) 529–540
ENERGY CONVERSION & MANAGEMENT
www.elsevier.com/locate/enconman

Thermal behaviour of solar air heater with compound parabolic concentrator

Réné Tchinda *

IUT Fotso Victor, University of Dschang, P.O. Box 134, Bandjoun, Cameroon
ICTP Strada Costiera 11, 34014 Trieste, Italy

Received 5 January 2007; received in revised form 25 July 2007; accepted 19 August 2007
Available online 24 October 2007

Abstract

A mathematical model for computing the thermal performance of an air heater with a truncated compound parabolic concentrator having a flat one-sided absorber is presented. A computer code that employs an iterative solution procedure is constructed to solve the governing energy equations and to estimate the performance parameters of the collector. The effects of the air mass flow rate, the wind speed and the collector length on the thermal performance of the present air heater are investigated. Predictions for the performance of the solar heater also exhibit reasonable agreement, with experimental data with an average error of 7%.

Keywords: CPC collector; Flat one-sided absorber; Air heating; Optical efficiency; Mass flow rate; CPC length

1. Introduction

Simulation models are important design tools and are useful for predicting the collector's experimental performance. In any solar energy application, it would be desirable to analyse theoretically any given system as extensively as possible before embarking on the construction of one for installation. Rabl [20], Hsieh [12], Prapas et al. [19], Norton et al. [15], Eames and Norton [6] and Oommen and Jayaraman [17] analysed non-evacuated CPC cavities with flat or cylindrical absorbers. The thermal analyses of such collectors have been well documented [9,23,24]. However, a close examination of the papers reveals that the case of a cylindrical absorber is of particular interest because standard piping and evacuated tubes are commonplace receiver elements, and because the cylindrical shape reduces thermal losses through the back of the collector. Other CPC configurations like the non-evacuated stationary CPC solar collector with flat bi-facial absorber [26], the CPC augmented with a reverse flat plate absorber [7] and an asymmetric compound parabolic concentrator [1,8,13] have been proposed. Papers reporting thermal analysis of the CPC with flat one-sided absorber are rarely found, and those published are devoted to the effect of truncation on the optical, thermal losses and collectible energy [3] or to increasing the electrical energy output [10]. Recently, Pramuang and Exell [18] reported the results of an experimental study in which the method of Chung-paibulpatana and Excell is used to determine the collector parameters of a solar flat plate collector with a CPC for heating air.

The purpose of this paper is to quantify the heat transfer within compound parabolic concentrating solar energy collectors with a flat one-sided absorber. A mathematical model analysing the collector thermal performance is introduced and examined by using a constructed computer code that uses an iterative procedure.

2. Structure of CPC and mathematical modeling

The CPC is capable of accepting solar radiation for long periods each day without diurnal tracking of the sun. It

* Tel.: +237 985 8481; fax: +237 344 5814.
E-mail address: ttchinda@yahoo.fr

0196-8904/$ - see front matter © 2007 Elsevier Ltd. All rights reserved.
doi:10.1016/j.enconman.2007.08.004

Nomenclature

A	area (m^2)
C_p	specific heat (J/kg K)
C_a	geometric concentrator ratio
e	thickness (m)
h	heat transfer coefficient (W/m^2 K)
I	solar intensity (W/m^2)
L	length of tube (m)
l	breadth (m)
M	mass based on unit aperture area (kg/m^2)
$\dot{m}$	mass flow rate (kg/s)
$\langle n \rangle$	number of reflections
q	heat flow (W/m^2)
T	temperature (K)
T_{fm}	$\left(\frac{1}{L}\int_0^L T_f(x,t)dx\right)$(K)
U_L	overall heat loss coefficient (W/m^2 K)

Greek letters

$\bar{\alpha}$	absorptance
$\bar{\rho}$	reflectance
$\bar{\tau}$	transmittance
σ	Stefan–Boltzman's constant (W/m^2 K^4)
μ	dynamic viscosity (kg/ms)
ε	emissivity
η	thermal efficiency
λ	thermal conductivity (W/ms)

Subscripts

b	ambient
c	cover
d	daily
e	inlet
o	outlet
p	flat one-sided absorber
s	sky
m	mirror
f	fluid

also has the advantage of concentrating the diffuse radiation, which is not possible using an imaging collector [18]. The two dimensional CPC collector with a flat absorber is the one studied experimentally by Pramuang and Exell [18]. The principal dimensions for the CPC collector used are labelled in Fig. 1 in both cross-section Fig. 1-a and side view Fig. 1-b.

In order to simplify the analysis, the following main assumptions are made:

A-1: It is assumed that the CPC is ideal and free from fabrication errors.

A-2: Any beam of radiation incident within the acceptance angle θ_a, with the help of the parabolic reflector can reach the receiver. The concentration ratio used in this work is defined on a geometrical basis and is expressed in terms of the total receiver area ($C_a = 1/\sin(\theta_a) = A_c/A_p$) [3,12].

A-3: The reflection of radiation from the parabolic reflector is taken into account by the apparent reflectance $\rho_m^{\langle n \rangle}$, with $\langle n \rangle = 0.5 + 0.07C_a$ for a CPC with flat plate absorber [21,23].

A-4: The direction of the beam radiation incident on various components in the collector can be found through geometry. Any reflection from these components, particularly multi-reflections from the parabolic reflector, will cause a reorientation of rays to the effect that the ray's reflection pattern becomes exceedingly difficult to follow without reliance on a detailed ray tracing. To facilitate analysis, these reflections are treated as diffuse, and their energy is taken into account in terms of diffuse reflectivities [12,23]. The succeeding absorption and transmission processes inside the CPC are diffusive and are taken into account in terms of the diffuse properties. The solar and infrared energy exchanges in the collector are treated separately using pertinent radiative properties in the spectrum.

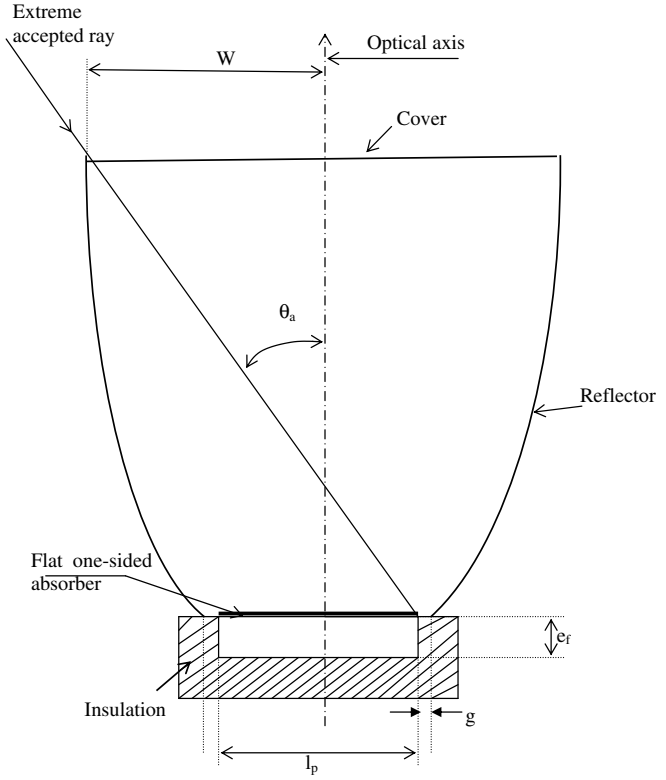

Fig. 1-a. A two dimensional CPC with a flat one-sided absorber. Cross section.

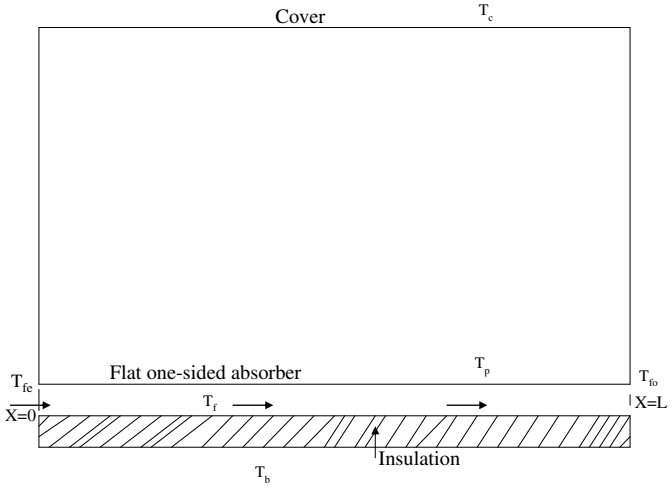

Fig. 1-b. A two dimensional CPC with a flat one-sided absorber. Side View.

A-5: The physical and optical properties of materials are assumed to be independent of temperature.

A-6: The concentrator does not produce an image of the light source, hence it is called a non-imaging concentrator.

Fig. 1-c illustrates the electric analogy circuit for the CPC collector. Applying heat balances in a suitable way, the following set of partial differential equations can be derived:

For the cover

$$M_c C_{pc} \frac{\partial T_c}{\partial t} = q_c(t) + h_{Rp}(T_p - T_c) + h_{p/c}(T_p - T_c) - h_{Rs}(T_c - T_s) - h_{c/a}(T_c - T_b) \quad (1)$$

with $t > 0$.

For the flat absorber

$$M_p C_{pp} \frac{\partial T_p}{\partial t} = q_p(t) - h_{Rp}(T_p - T_c) - h_{p/c}(T_p - T_c) - q_u(t) \quad (2)$$

with $t > 0$.

In Eqs. (1) and (2), $q_c(t)$ and $q_p(t)$ have been expressed using Hsieh's theory [23], as:

$$q_c(t) = I(t)\left[\bar{\alpha}_c + \bar{\alpha}_c \bar{\tau}_c \bar{\rho}_p \rho_m^{2\langle n\rangle}\right] \frac{A_c}{A_p} \quad (4)$$

$$q_p(t) = I(t)\bar{\tau}_c \rho_m^{\langle n\rangle} P\left[\bar{\alpha}_p + \bar{\alpha}_p \bar{\rho}_p \bar{\rho}_c \frac{A_p}{A_c}\right] \frac{A_c}{A_p} \quad (5)$$

P is the gap loss factor, which is equal to $1 - g/l_p$ [21], where g is the gap thickness. $A_c = W*L$ and $A_p = l_p*L$.

At any point x, the fluid temperature (T_f) is related to the useful energy q_u (see Eqs. (2) and (3)) and the absorber temperature (T_p) by the following expression:

$$q_u = U_f(T_p - T_f) \quad (6)$$

The factor U_f is the convective heat transfer coefficient between the heat transfer fluid and the walls of the absorber. It is calculated from the relationship:

$$U_f = \frac{N_{uf}\lambda_f}{D_H} \quad (7)$$

where the Nusselt number N_u and the hydraulic diameter D_H are given in Appendix A.

Since the absorptance of the cover and the thermal capacities of the components of the collector are small, we neglect them. However, the functioning of the collector remains variable with time because it depends on the unsteady solar intensity. Eliminating T_c and T_p from the simplified equations obtained, one gets:

$$C_{pf}\dot{m}\frac{dT_f}{dx} = l_p[S_p - U_L(T_f - T_b)]F' \quad (8)$$

with

$$S_p = I(t)\bar{\tau}_c \rho_m^{\langle n\rangle} P\left[\bar{\alpha}_p + \bar{\alpha}_p \bar{\rho}_p \bar{\rho}_c \frac{A_p}{A_c}\right] \frac{A_c}{A_p} + \frac{(h_{Rp} + h_{p/c})\left(I(t)\left[\bar{\alpha}_c + \bar{\alpha}_c \bar{\tau}_c \bar{\rho}_p \rho_m^{2\langle n\rangle}\right]\frac{A_c}{A_p}\right)}{h_{Rp} + h_{p/c} + h_{Rs} + h_{c/a}} - \frac{(h_{Rp} + h_{p/c})\Delta T h_{Rs}}{h_{Rp} + h_{p/c} + h_{Rs} + h_{c/a}} \quad (9)$$

$$U_L = \frac{(h_{Rp} + h_{p/c} + h_{Rs} + h_{c/a})(U_0U_f + U_0h_{Rp} + U_0h_{p/c} + h_{Rp}U_f + h_{p/c}U_f) + (U_0 - U_f)(h_{Rp} + h_{p/c})^2}{(h_{Rp} + h_{p/c} + h_{Rs} + h_{c/a})U_f} \quad (10)$$

For the fluid

$$\rho_f e_f C_{pf}\frac{\partial T_f}{\partial t} = q_u(t) - \frac{\dot{m}C_{pf}}{l_p}\frac{\partial T_f}{\partial x} - U_0(T_f - T_b) \quad (3)$$

with $t > 0$ and $0 < x < L$.

$$F' = \frac{U_f(h_{Rp} + h_{p/c} + h_{c/a} + h_{Rs})}{(h_{Rp} + h_{p/c} + h_{c/a} + h_{Rs})(h_{Rp} + h_{p/c} + U_f) - (h_{Rp} + h_{p/c})^2} \quad (11)$$

To evaluate the collector's performance, it is necessary to estimate the overall loss coefficient U_L, the collector efficiency factor F' and the internal heat transfer coefficients.

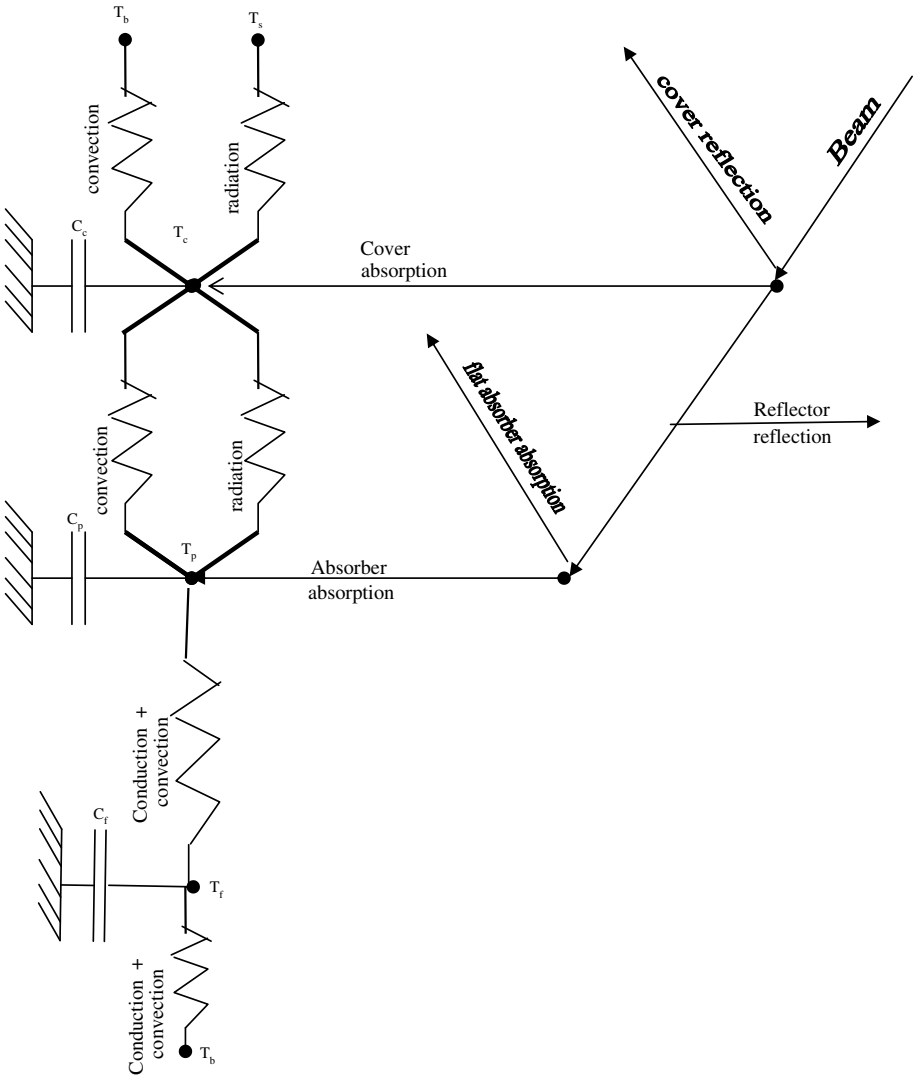

Fig. 1-c. A two imensional CPC with a flat one-sided absorber.

The relations determined for the various heat transfer coefficients are presented in Appendix A.

Assuming that the overall heat loss coefficient U_L and the collector efficiency factor are temperature independent in position, the efficiency is found to be:

$$\eta_{inst} = \frac{Q_u}{A_C I(t)} \tag{12}$$

where the useful thermal power Q_u extracted from the CPC collector is calculated from the relationship:

$$Q_u = F_R A_r \{S_p - U_L(T_{fe}(0,t) - T_b(t))\} \tag{13}$$

F_R is a removal factor given by:

$$F_R = \frac{C_{pf}\dot{m}}{l_p L U_L}\left(1 - e^{\left(\frac{-l_p L F' U_L}{C_{pf}\dot{m}}\right)}\right) \tag{14}$$

Using Eqs. (12) and (13), η_{inst} becomes:

$$\eta_{inst} = (\eta_0 + F_A)F_R - \frac{U_L}{C_a I(t)} F_R (T_{fe}(0,t) - T_b(t)) \tag{15}$$

where the optical efficiency is given by:

$$\eta_0 = \bar{\tau}_c \rho_m^n \bar{\alpha}_p P\left(1 + \bar{\rho}_p \rho_c \frac{l_p}{2W}\right) \tag{16-a}$$

According to Rabl et al. [22] and to Pramuang and Exell [18], the optical efficiency is given by:

$$\eta_{01} = \bar{\tau}_c \rho_m^{\langle n \rangle} \bar{\alpha}_p \tag{16-b}$$

Table 1
The characteristics of the CPCs

Parameter	Symbol	Units	Value
Acceptance half angle	θ_a	°	15
Cover absorptance	$\bar{\alpha}_c$	/	0.05
Flat plate absorber absorptance	$\bar{\alpha}_p$	/	0.95
Cover transmittance	$\bar{\tau}_c$	/	0.89
Cover emittance	ε_c	/	0.85
Flat plate absorber emittance	ε_p	/	0.91
Cover reflectance	$\bar{\rho}_c$	/	0.05
Reflector reflectance	ρ_m	/	0.86
Flat plate absorber reflectance	$\bar{\rho}_p$	/	0.15

The optical efficiency determined from direct measurements [18] of the optical properties of the materials listed in Table 1 using Eqs. (16-a and 16-b) have values $\eta_0 \approx 0.72$ and $\eta_{01} \approx 0.75$, respectively. However, the result of Pramuang and Exell [18] obtained using Eq. (16-b) is different. The difference is due to the fact that in the numerical calculation of Pramuang and Exell [18], the number of reflections is computed using the relation $\langle n \rangle = 1 + 0.07 C_a$ which is a relation used for a CPC with tubular absorber [21]. The analytical results of Eq. (16-a) agree with the optical efficiency found by direct measurements ($\eta_0 = 0.67$, see Pramuang and Exell [18] with an error of 7%. Comparing Eqs. (16-a) and (16-b), the ratio gives:

$$\frac{\eta_0}{\eta_{01}} = P\left(1 + \bar{\rho}_p \rho_c \frac{l_p}{2W}\right) < 1 \tag{17}$$

An examination of this equation, when $P \to 1$ ($g \to 0$, corresponding to a case where the reflector touches the receiver) shows that Eq. (16-a) agrees with Eq. (16-b) with an average error of 1%. In many solar thermal applications, however, it is necessary to have $g \neq 0$ ($P < 1$), because a gap between the reflector and the absorber is needed to reduce conductive heat losses. The above result shows that a gap between the reflector and the absorber causes optical losses, but a compromise between optical and thermal performance must be made.

In Eq. (15), F_A is named the enclosure absorption factor [23]. It is given by the relationship:

$$F_A = \frac{(h_{Rp} + h_{p/c})}{(h_{Rp} + h_{p/c} + h_{c/a} + h_{Rs})} \left\{ \bar{\alpha}_c + \bar{\alpha}_c \bar{\tau}_c \bar{\rho}_p \rho_m^{2\langle n \rangle} - \frac{\Delta T h_{Rs}}{I(t) C_a} \right\} \tag{18}$$

The performance of the system over a period of a day is computed as the daily average efficiency:

$$\eta = \frac{\int_{t_r}^{t_s} \dot{m} C_{pf} (T_{f0}(L,t) - T_{fe}(0,t) \mathrm{d}t}{A_c \int_{t_r}^{t_s} I(t) \mathrm{d}t} \tag{19}$$

where $t_r = 6$ a.m. and $t_s = 6$ p.m.

3. Calculation procedure

In the numerical calculations, an iterative method is used to take into account the effect of the temperature dependence of the various heat transfer coefficients. For certain temperatures, they are first calculated by using the standard expressions given earlier. The equations are solved by assuming the coefficients constant, and the solutions are used to generate all the heat transfer coefficients again and the iteration continues until the values converge. The convergence criteria are given by the following relationship:

$$\mathrm{Sup}\left[\max_i \left| T_{xi}^{k+1} - T_{xi}^{k} \right|, \left| T_c^{k+1} - T_c^{k} \right|, \left| T_p^{k+1} - T_p^{k} \right| \right] \leqslant \gamma \tag{20}$$

An appropriate choice of γ is important to make sure that the convergence is rich. Several tests have been made for which γ was taken as 10^{-3}, 10^{-4} and 10^{-5} and the resulting values and numbers of iterations were compared. The results showed that for the low value of flux ($I(t) < 270$ W/m^2), the value $\gamma = 10^{-3}$ was satisfactory, while for the higher values of flux $I(t)$, $\gamma \sim 8 \times 10^{-4}$ was adequate. The value of γ was kept constant, at 10^{-5}, throughout the present calculations. The computer program is based on FORTRAN and proceeds as outlined above.

4. Physical parameters

One collector panel with CPC collectors truncated to one-third of the full size within the acceptance half angle of 15° is considered. The collector has a total aperture area of 0.72 m^2 and a flat plate absorber area of 0.24 m^2. This collector has overall dimensions of 0.6 m height, 0.6 m width, 8 mm gap thickness, and the calculations are done for three values of CPC length, L, from 1.2 to 2 m. The receiving surface, which is painted non-selective matte black, forms the upper side of a rectangular air flow duct of depth 0.03 m made of aluminium sheet 0.2 mm thick [18]. The bottom of the duct is insulated with fibre glass 0.05 m thick. The optical properties of the materials in the collector are listed in Table 1. The physical properties of air were assumed to vary linearly with temperature within the range encountered in solar air heaters. Therefore, typical linear equations for the viscosity, density, thermal conductivity and specific heat of air were implemented in the theoretical procedure. The following are recalled in Appendix A. The mean values of the ambient temperature and global radiation in May at Garoua in Cameroon (9°20′ N; 13°23′ E; altitude 241 m) are used [25].

5. Results and discussion

A series of runs with individual parameters varied while others are held constant were conducted and analysed to investigate the influence of these parameters on the thermal performance of the present model. The effect of increasing the volume flow rate on the local air, air outlet, absorber plate and cover temperatures and the instantaneous and daily average efficiencies is presented in Figs. 2 to 5. It is apparent, as expected, that as the air mass flow rate increases, the air flow local temperature and air outlet temperature decreases. Further, for high mass flow rates, the collector operating temperature would be lower, resulting in lower heat losses and, subsequently, higher efficiencies. In all the results, it is observed that the absorber plate exhibits the highest temperature and the cover the lowest. As the air flow rate increases, the temperature differences between the air and the absorber plate decrease. The effects of wind on the instantaneous and daily efficiencies are shown in Figs. 4-a and b. The results show that by decreasing the value of the wind speed, as expected, the wind heat transfer coefficient decreases, and thus, the overall loss coefficient value and the instantaneous and daily efficiencies increased.

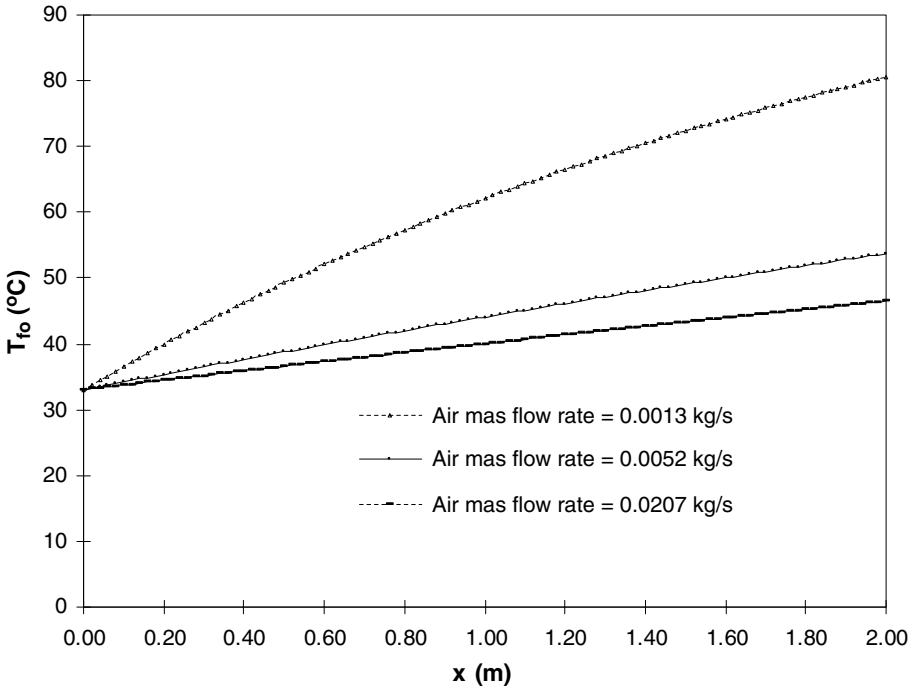

Fig. 2-a. Effect of the air mass flow rate on the local temperature in the flow direction; $L = 1.2$ m, $T_{fe} = 33$ °C, $v = 3.0$ m/s.

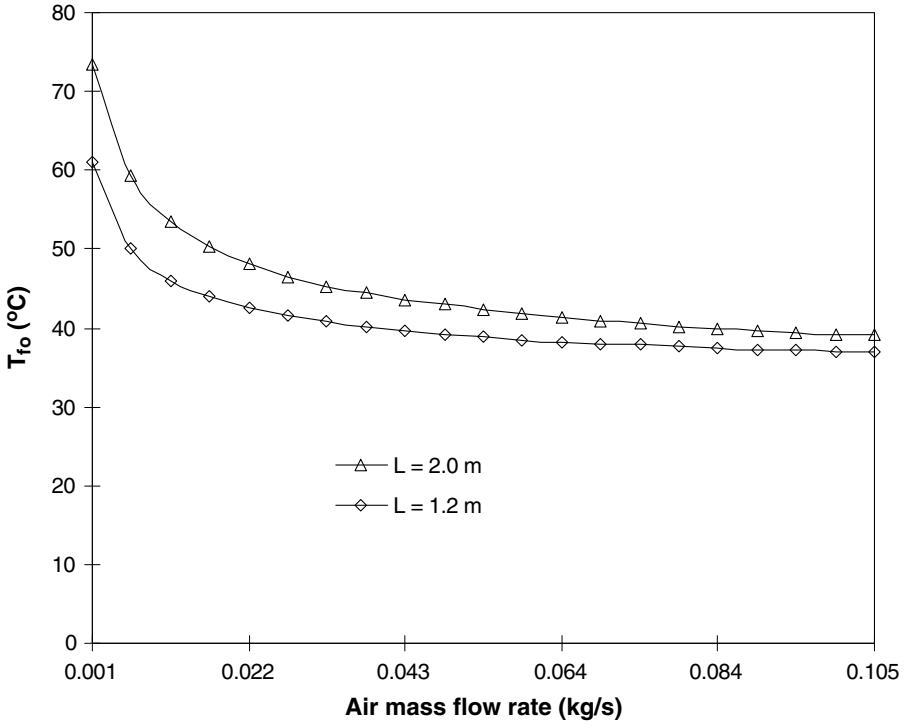

Fig. 2-b. The outlet air temperature at $t_M = 12.30$ p.m. as a function of the mass flow rate for some values of L.

The effect of increasing the collector length on the thermal performance is displayed in Figs. 2-a and 5. It can be seen that as the collector length is increased, the absorber average temperature is appreciably increased, as was the air temperature. However, the instantaneous and daily average efficiencies slightly decrease with the increase in length of the collector, which presumably results from the greater heat losses to the surroundings since both the average absorber temperature and the size of the collector are increased.

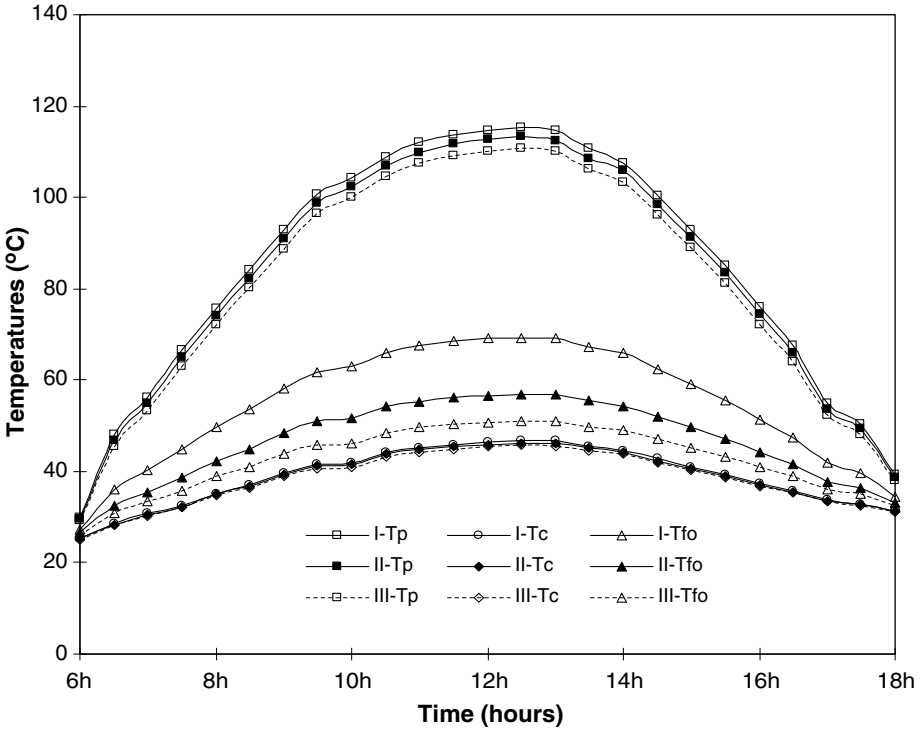

Fig. 3. Effect of the air mass flow rate on the hourly variations of temperatures of the collector, **I**-air mass flow rate = 0.0013 kg/s; **II**-air mass flow rate = 0.0065 kg/s; **III**-air mass flow rate = 0.013 kg/s, $L = 2.0$ m.

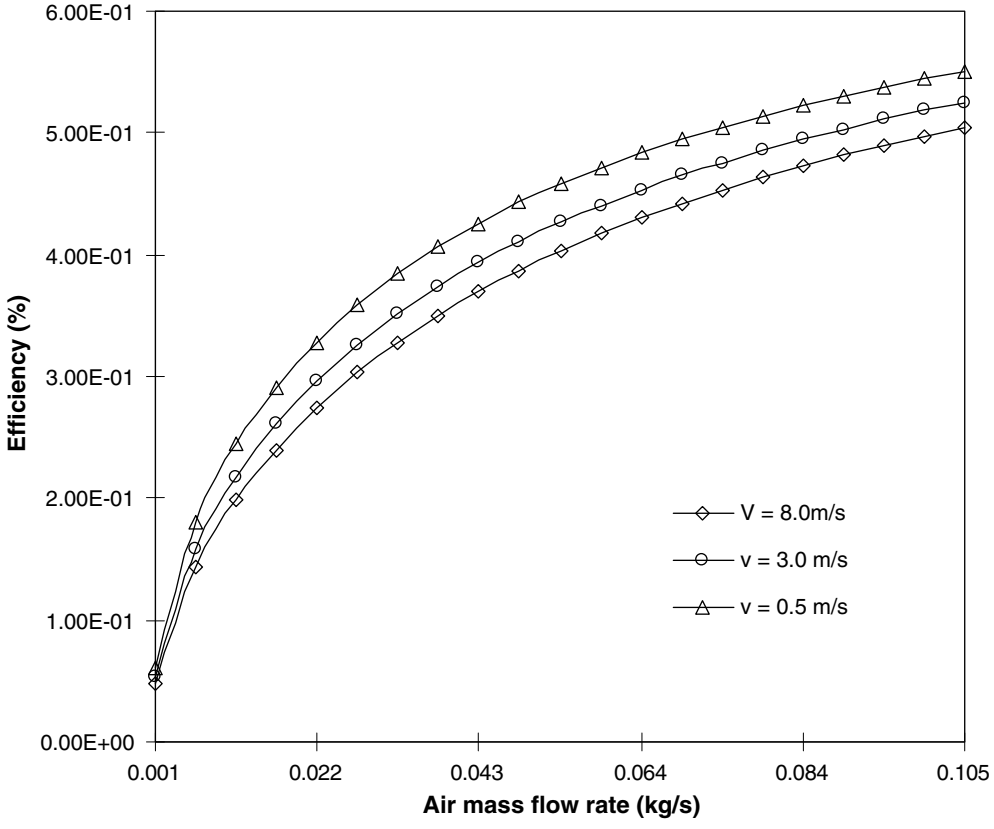

Fig. 4-a. Graph of the instantaneous efficiency numerical results for three wind speeds.

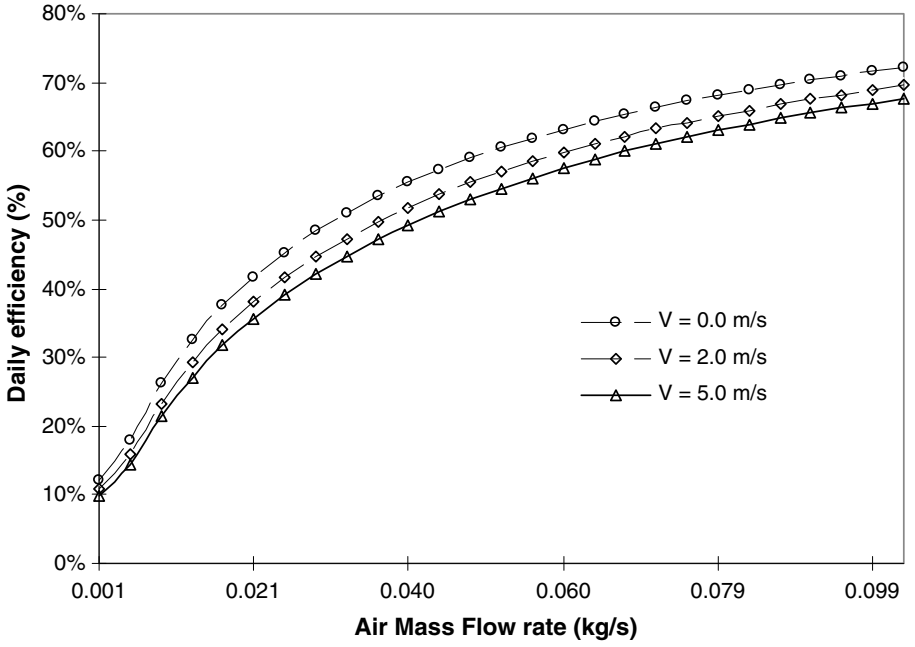

Fig. 4-b. Effect of the air mass flow rate on the dailly efficiency for three values of wind speed, $L = 1.2$ m, $T_{fe} = 33$ °C.

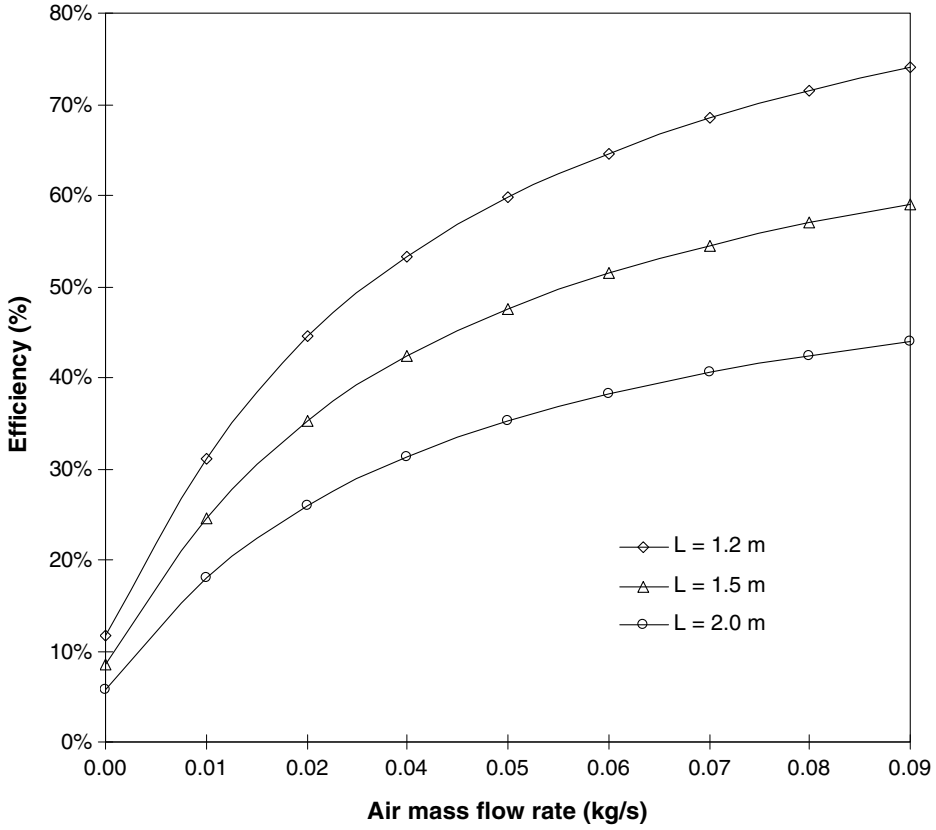

Fig. 5-a. Effect of the air mass flow rate on the daily efficiency of the collector for three values of L.

Fig. 6 shows the instantaneous efficiency calculated for different solar irradiances.

Fig. 7 shows the effect of the air mass flow rate on U_L and F'. It is shown that the collector efficiency factor F' increases with the air mass flow rate. It is also observed, as expected, that U_L decreases with the increase of the air mass flow rate.

Fig. 8 compares the efficiency obtained from the present mathematical model and the experimental data

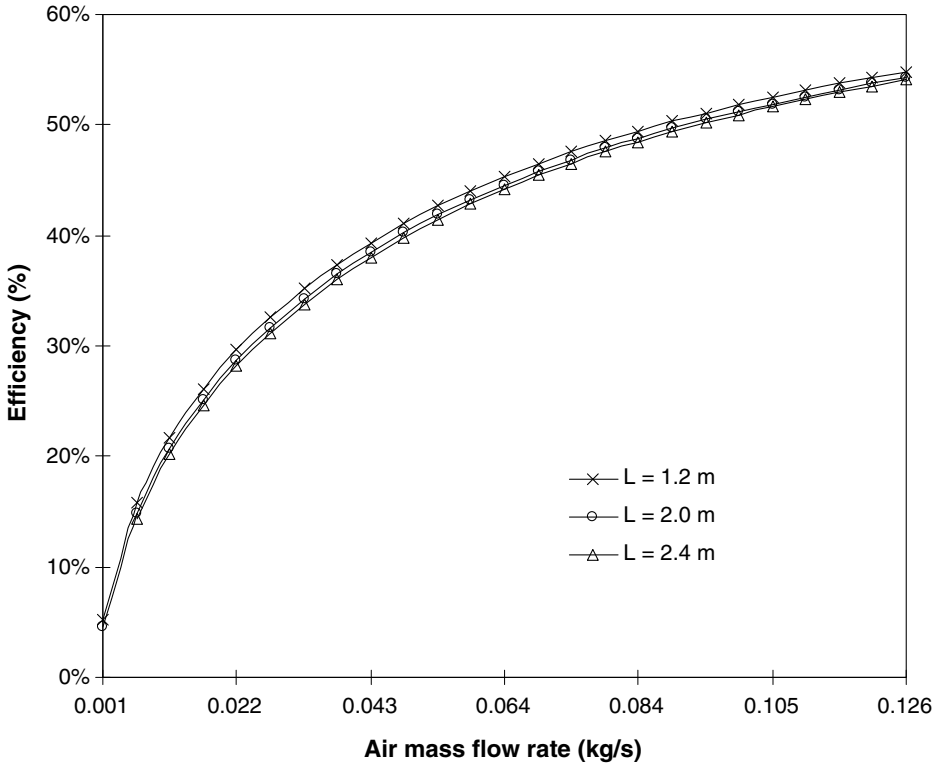

Fig. 5-b. Effect of the air mass flow rate and collector length on the instantaneous efficiency at $t_M = 12.30$ p.m.

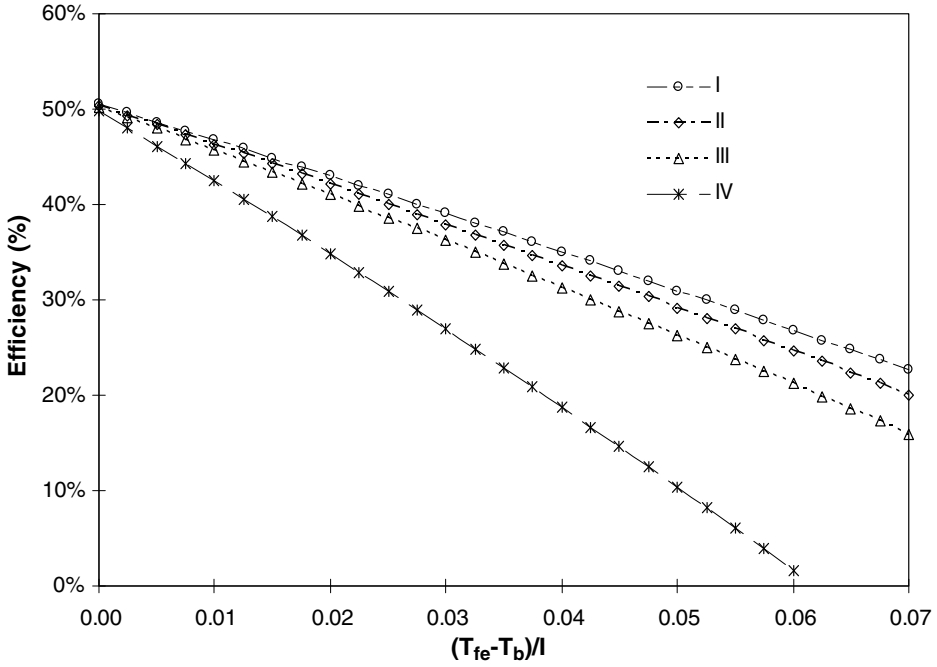

Fig. 6. Collector efficiency curves calculated for fourth values of global radiation: (I) $\mathbf{I} \sim 951$ W/m^2; (II) $\mathbf{I} \sim 815$ W/m^2; (III) $\mathbf{I} \sim 636$ W/m^2; (IV) $\mathbf{I} \sim 327$ W/m^2; $v = 3{,}0$ m/s, air mass flow rate $\sim$0.09 kg/s.

of Pramuang and Exell [18]. The test data have been taken from a collector having conditions sufficiently close to those given by Pramuang and Exell [18]. It can be seen that the results obtained show good agreement with the experimental data, with an average error of 8%.

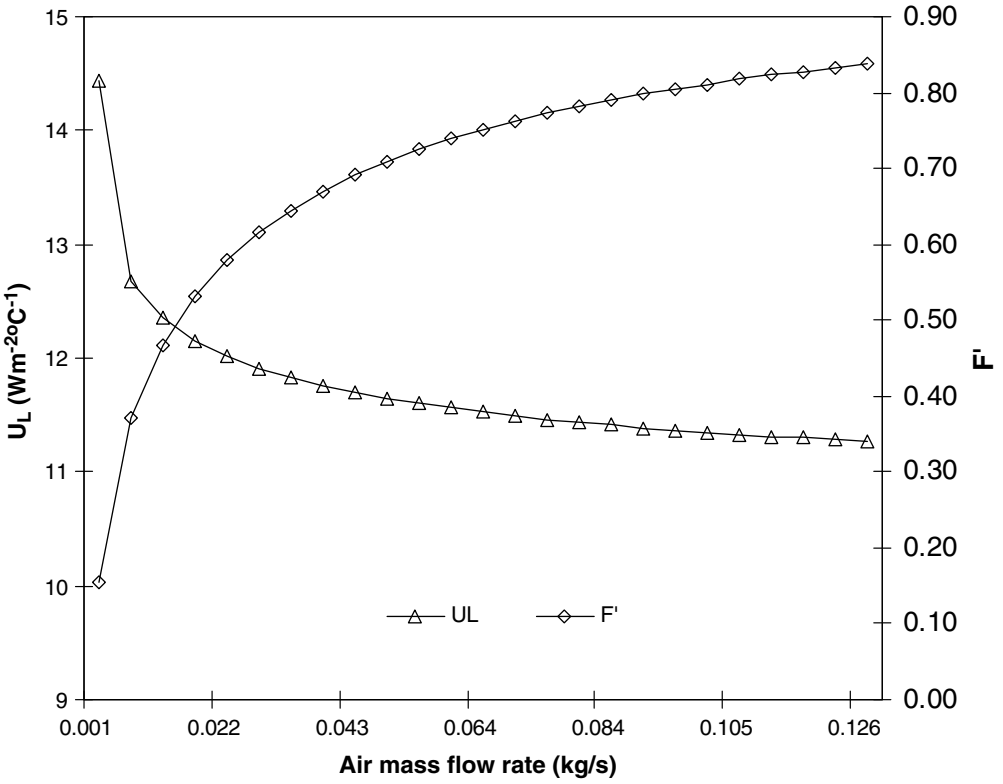

Fig. 7. Effect of the air mass flow rate and collector length on F' and U_L.

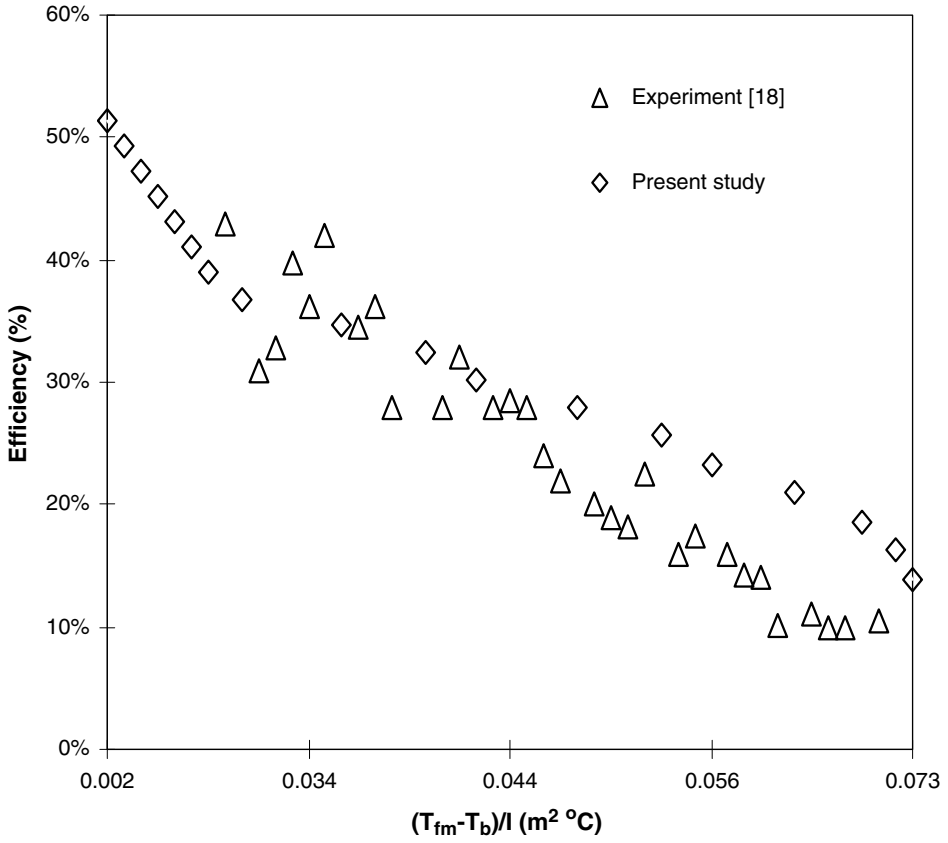

Fig. 8. Comparison of the collector efficiencies.

6. Conclusion

The heat transfer characteristics and thermal performance of a solar flat plate collector with a CPC has been presented. A theoretical solution procedure of the energy equations using a computer code for predicting the thermal performance of the present solar air heater has been made. The influence of the air mass flow rate, collector length and wind speed on the performance of the present air heater has been discussed. Reasonable agreement is obtained from the comparison between the numerical results and experimental data.

Acknowledgement

This work was done within the framework of the Associateship Scheme of ICTP. Financial support from the Swedish International Development Cooperation Agency is also acknowledged.

Appendix A

The different heat transfer coefficients for each surface in the present system are evaluated as follows.

Radiation heat transfer from the cover to the Sky

The radiative h_{Rp} heat transfer coefficient between the flat plate absorber and the cover is:

$$h_{Rp} = \frac{\sigma\left(T_p^2 + T_c^2\right)(T_p + T_c)}{\frac{1}{\varepsilon_p} + \frac{A_p}{A_c}\left(\frac{1}{\varepsilon_c} - 1\right)} \tag{A1}$$

Radiation heat transfer from the flat plate absorber to the cover

The radiative heat loss coefficient h_{Rs} between the cover and the sky is calculated from the relationship:

$$h_{Rs} = \sigma\varepsilon_c\left(T_c^2 + T_s^2\right)(T_c + T_s)\frac{A_c}{A_p} \tag{A2-a}$$

where the expression of the sky temperature is given by Hsieh [11,12,24]:

$$T_s = T_b - 6 \tag{A2-b}$$

Convection heat transfer coefficient from the cover due to wind

The heat loss coefficient by convection $h_{c/a}$ between the cover and the ambient is correlated by Duffie and Beckman [4] as:

$$h_{c/a} = (5.7 + 3.8v)\frac{A_c}{A_p} \tag{A3-a}$$

or by Watmuff et al. [27] as:

$$h_{c/a} = (2.8 + 3.3v)\frac{A_c}{A_p} \tag{A3-b}$$

where v is the wind velocity. The Duffie and Beckman correlation was the one that was employed in this study.

Convective heat transfer coefficient between flat plate absorber and cover

According to the Hsieh theory [12,23], the convective $h_{p/c}$ heat transfer between the flat plate absorber and the cover is:

$$h_{p/c} = \left(3.25 + 0.0085\frac{T_p - T_c}{2D_H}\right)\frac{A_c}{A_p} \tag{A4-a}$$

where

$$D_H = \frac{2l_p e_f}{l_p + e_f} \tag{A4-b}$$

The flow is assumed to be hydrodynamically fully developed at the collector inlet. The inner surface convective heat transfer coefficients were modelled according to the flow regime.

- For laminar flow ($R_e < 2100$) by the Mercer correlation [2,14]

$$N_u = 4.9 + \frac{0.0606(R_e P_r D_H/L)^{1.2}}{1 + 0.0909(R_e P_r D_H/L)^{0.7} P_r^{0.17}} \tag{A-4}$$

- For turbulent flow ($R_e > 2100$) by the Kays correlation presented in a mathematical form by Duffie and Beckman [5].

$$N_u = 0.0158 R_e^{0.8} \tag{A-5}$$

with

$$R_e = \frac{\dot{m} D_H}{l_p e_f \mu_f}, \quad P_r = \frac{\mu_f C_f}{\lambda_f} \tag{A-6}$$

Physical properties of air [16]

$$\text{Viscosity} : \mu = [1.983 + 0.00184(T - 27)]10^{-5} \tag{A-7}$$

$$\text{Density} : \rho = 1.1774 - 0.00359(T - 27) \tag{A-8}$$

$$\text{Thermal Conductivity} : \lambda = 0.02624 + 0.0000758(T - 27) \tag{A-9}$$

$$\text{Specific heat} : C_p = 1.0057 + 0.000066(T - 27) \tag{A-10}$$

References

[1] Adsten M, Hellström B, Karlsson B. Measurement of radiation on the absorber in an asymmetric CPC collector. Sol Energy 2004;76:199–206.
[2] Brodkey RS, Hershey HC. Transport Phenomena. McGraw-Hill Book Company; 1988.
[3] Carvalho MJ, Collares-Pereira M, Gordon JM, Rabl A. Truncation of CPC solar collectors and its effect on energy collection. Sol Energy 1985;35(5):393–9.

[4] Duffie JA, Beckman WA. Solar energy thermal processes. New York: Wiley; 1974. pp. 83.
[5] Duffie JA, Beckman WA. Solar engineering of thermal processes. New York: John Wiley and Sons; 1980.
[6] Eames PC, Norton B. Validated, unified model for optics and heat transfer in line- axis concentrating solar energy collectors. Sol Energy 1993;50(4):339–55.
[7] Eames PC, Smyth M, Norton B. The experimental validation of a comprehensive unified model for optics and transfer in line-axis solar energy systems. Sol Energy 2001;71:121–33.
[8] Fang Y, Eames PC, Hyde TJ, Norton B. Thermal performance of complex multimaterial frames for evacuated glazing. ISES solar world congress, 14th to 19th June 2003, Goteborg, Sweden.
[9] Fraidenraich N, Lima DERFDE, Tiba C, Barbosa EM. Simulation model of CPC collector with temperature dependent heat loss coefficient. Sol Energy 1999;65(2):99–110.
[10] Gordon JM. Ideal solar concentrators for photoelectrochemical cells. Sol Energy 1988;40(4):391–5.
[11] Hsieh CK. Design of system using CPC collectors to collect solar energy and to produce industrial process steam. Argonne national laboratory, Rep ANL 1979:79–102.
[12] Hsieh CK. Thermal analysis of CPC collectors. Sol Energy 1981;27:19–28.
[13] Mallick TK, Eames PC, Hyde TJ, Norton B. The design and experimental characterisation of an asymmetric compound parabolic photovoltaic concentrator for buiding façade integration in the UK. Sol Energy 2004;77:319–27.
[14] Mercer WE, Pearce WM, Hichcock JE. Laminar forced convection in the entrance region between parallel flat plates. J Heat Trans-T, ASME 1967;89:251–7.
[15] Norton B, Prapas DE, Eames PC, Probert SD. Measured performance of curved inverted-vee, absorber compound parabolic concentrating solar energy collectors. Sol Energy 1989;43(5):267–79.
[16] Ong KS. Thermal performance of solar air heaters: mathematical model and solution procedure. Sol Energy 1995;55(2):93–109.
[17] Oommen R, Jayaraman S. Development and performance analysis of compound parabolic solar concentrators with reduced gap losses-oversized reflector. Energy Convers Manage 2001;42: 1379–99.
[18] Pramuang S, Exell RHB. Transient test of a solar air heater with a compound parabolic concentrator. Renew Energy 2005;30:715–28.
[19] Prapas DE, Norton B, Probert SD. Thermal design of compound parabolic concentrating solar energy collectors. J Solar Energy Eng 1987;109:161–8.
[20] Rabl A. Optical and Thermal properties of compound parabolic concentrators. Sol Energy 1976;18:497–511.
[21] Rabl A, Goodman NB, Winston R. Practical design considerations for CPC solar collectors. Sol Energy 1979;22:373–81.
[22] Rabl A, O'Gallagher J, Winston R. Design and test of non-evacuated solar collector with compound parabolic concentrator. Sol Energy 1980;25:335–51.
[23] Tchinda R.'Contribution à l'étude des transferts de chaleur dans les systèmes de conversion thermique de l'énergie Solaire: cas des Concentrateurs paraboliques composés',Thèse de Doctorat d'Etat, Université de Yaoundé I, 2003, pp. 209.
[24] Tchinda R, Kaptouom E, Njomo D. Study of the CPC collector thermal behaviour. Energy Convers Manage 1998;39(13): 1395–406.
[25] Tchinda R, Kaptouom E. Simulation Numérique des Performances d'un Distillateur Solaire Fonctionnant en Mode Indirect. African J Sci Technol 2004:79–91.
[26] Tripanagnostopoulos Y, Yianoulis P, Papaefthimiou S, Zafeiratos S. CPC solar collector with bifacial absorbers. Sol Energy 2000;69(3):191–203.
[27] Watmuff JH, Carters WWS, Proctor D. Solar and wind induced external coefficients for solar collectors. COMPLESW 1977;2:56.